Surface Impedance Absorbing Boundary for Terminating FDTD Simulations

Yunlong Mao [1,2], Atef Z. Elsherbeni [2], Si Li [1,2], and Tao Jiang [1]

[1] College of Information and Communication Engineering
Harbin Engineering University, Harbin, 150001 China
maoyunlong@hrbeu.edu.cn, jiangtao@hrbeu.edu.cn, lisi@hrbeu.edu.cn

[2] Department of Electrical Engineering and Computer Science
Colorado School of Mines, Golden, 80401, USA
aelsherb@mines.edu

Abstract **—** An Absorbing Boundary Condition (ABC) for FDTD simulations based on the concept of surface impedance boundary, which is referred to as Surface Impedance Absorbing Boundary Condition (SIABC), is proposed in this paper. It is extremely easy to implement relative to other absorbing boundaries and is found to be sufficient for many practical applications. The formulation of the SIABC is developed and implemented. The performance of SIABC is comparable with that of 10-layers CPML.

Inedx Terms **—** ABC, CPML, FDTD, SIABC.

I. INTRODUCTION

Since the moment it was introduced, absorbing boundary condition is widely used in the simulation of electromagnetic problems. Many absorbing boundaries are developed in the past years, like Engquist-Majda' ABC [1], Mur's ABC [2], PML [3], and CPML [4]. Engquist-Majda's ABC, along with Mur's ABC, are developed from wave equations. These ABCs are acceptable in 1D and 2D problems, but not usually very effective in 3D problems. Besides, a sufficiently far distance between the boundaries and the objects inside the computational domain is needed. Both PML and CPML, which are the most widely used nowadays, are developed by setting the impedance of ABCs' layers the same as that of free space. Thus, there won't be significant reflections back into the problem space, while a small distance between the objects and the boundaries is used. However, even though PML and CPML have great performance in 1D, 2D, and 3D problems, these two ABCs are not easy to implement and extra storage requirements are needed.

In 1997, Senior et al [5] presented the connection between Rytov's surface impedance boundary conditions [6] and Engquist-Majda's absorbing boundary conditions in partial differential equations (PDE) form. However, since the method is developed from the very old ABC which is no longer used in most cases, the performance of this method is not so good especially in 3D problems, compared to PML or CPML. Besides, it can only be applied to curvilinear/double-curved surfaces. In spite of these disadvantages, this is the first time to the best of our knowledge that surface impedance boundary conditions are tried as ABC for FDTD simulations.

In most FDTD simulations, the outer absorbing boundary conditions are planar surfaces, where Leontovich's surface impedance boundary condition [7] is suitable. In 1992, Maloney [8] and John Beggs [9] both successfully implemented Leontovich's surface impedance boundary condition with FDTD method, but not as an absorbing boundary. Thus, it is possible to construct a new absorbing boundary condition by setting the surface impedance of Leontovich's surface to that of free space in order to terminate

the outer boundary of the FDTD computational domain.

In this paper, this new absorbing boundary condition, which is referred to as Surface Impedance Absorbing Boundary Condition (SIABC), is introduced. Formulas for SIABC in 1D, 2D and 3D are derived and implemented with FDTD method. To verify the accuracy of this SIABC, a few examples are given, and the results are compared to those based on CPML in 3D, and PML in 1D configurations.

II. FORMULATION

Leontovich's surface impedance boundary conditions can be represented as:

$$\vec{E} = Z_s(\omega)\left[\vec{n} \times \vec{H}\right], \qquad (1)$$

where $\vec{E}$ is the electric field, and $\vec{H}$ is the magnetic field parameter. $Z_s(\omega)$ refers to the surface impedance of the interface, while $\vec{n}$ is the normal vector.

Equation (1) describes the relationship of electric field and magnetic field on the interface of two regions. If the wave propagate from free space into another free space, then the impedance of the interface should be:

$$Z_s(\omega) = Z_0 = \sqrt{\frac{\mu_0}{\epsilon_0}}, \qquad (2)$$

where μ_0 and ϵ_0 are the free space permeability and permittivity, respectively.

A. 3D SIABC formulation

The setup of SIABC for a 3D problem space is illustrated in Fig. 1, where SIABC is applied to all 6 boundaries.

In a 3D problem, the inward normal vector $\vec{n}$ can be rewritten as:

$$\vec{n} = c_x \vec{e_x} + c_y \vec{e_y} + c_z \vec{e_z}, \qquad (3)$$

where $\vec{e_x}, \vec{e_y}, \vec{e_z}$ are unit vectors of different directions, and c_x, c_y, c_z are the coefficients.

Substituting equation (3) into equation (1), and replacing $\vec{E}$ and $\vec{H}$ with:

$$\begin{cases} \vec{E} = E_x \vec{e_x} + E_y \vec{e_y} + E_z \vec{e_z}, \\ \vec{H} = H_x \vec{e_x} + H_y \vec{e_y} + H_z \vec{e_z}, \end{cases}$$

one can obtain that:

$$\begin{cases} E_x = Z_0\left[c_y H_z - c_z H_y\right], \\ E_y = Z_0\left[c_z H_x - c_x H_z\right], \\ E_z = Z_0\left[c_x H_y - c_y H_x\right]. \end{cases} \qquad (4)$$

The value of $\vec{n}$ is decided by the value of the coefficients c_x, c_y, c_z. When $\vec{n}$ is normal to any of the boundaries identified in Fig. 1, one of c_x, c_y, c_z should be '1' or '-1' meanwhile the other 2 are both '0'. Table 1 lists the values of c_x, c_y, c_z for different boundaries.
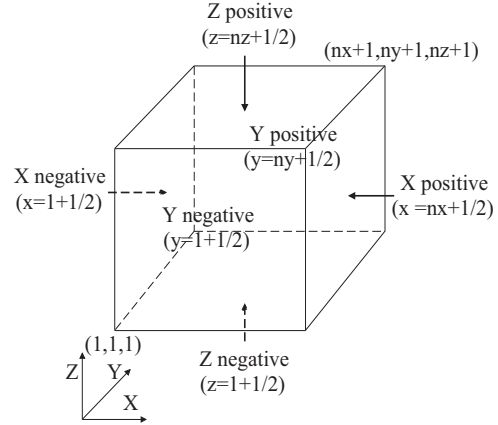

Fig. 1. Geometry of a 3D problem space with SIABC boundaries.

Table 1: Values of c_x, c_y, c_z for different boundaries

SIABC	c_x	c_y	c_z
$X_{negative}$	1	0	0
$X_{positive}$	-1	0	0
$Y_{negative}$	0	1	0
$Y_{positive}$	0	-1	0
$Z_{negative}$	0	0	1
$Z_{positive}$	0	0	-1

According to Maxwell's equations, in a source-free region,

$$\begin{cases} \dfrac{\partial H_x}{\partial t} = \dfrac{1}{\mu_x}\left(\dfrac{\partial E_y}{\partial z} - \dfrac{\partial E_z}{\partial y}\right), \\ \dfrac{\partial H_y}{\partial t} = \dfrac{1}{\mu_y}\left(\dfrac{\partial E_z}{\partial x} - \dfrac{\partial E_x}{\partial z}\right), \\ \dfrac{\partial H_z}{\partial t} = \dfrac{1}{\mu_z}\left(\dfrac{\partial E_x}{\partial y} - \dfrac{\partial E_y}{\partial z}\right). \end{cases} \qquad (5)$$

For the SIABC on the X negative boundary, according to Table 1, and as shown in Fig. 2, equation (4) becomes:

$$\begin{cases} E_y(1,j,k) = Z_0\left[-H_z(1,j,k)\right], \\ E_z(1,j,k) = Z_0\left[H_y(1,j,k)\right]. \end{cases} \qquad (6)$$

On this boundary, E_x is not needed as it is not tangential to the boundary. Then, we can substitute

equations (6) into equation (5), which yields:

$$
\begin{cases}
\dfrac{\partial H_x}{\partial t} = \dfrac{E_y(1,j,k+1) - E_y(1,j,k)}{\mu_x \triangle z} \\
\qquad - \dfrac{E_z(1,j+1,k) - E_y(1,j,k)}{\mu_x \triangle y}, \quad (7a) \\
\dfrac{\partial H_y}{\partial t} = \dfrac{E_z(2,j,k) - Z_0 H_y(1,j,k)}{\mu_y \triangle x/2} \\
\qquad - \dfrac{E_x(1,j,k+1) - E_x(1,j,k)}{\mu_y \triangle z}, \quad (7b) \\
\dfrac{\partial H_z}{\partial t} = \dfrac{E_x(1,j+1,k) - E_x(i,j,k)}{\mu_z \triangle y} \\
\qquad - \dfrac{E_y(2,j,k) + Z_0 H_z(1,j,k)}{\mu_z \triangle x/2}. \quad (7c)
\end{cases}
$$

Unlike the normal FDTD method, the electric fields, E_y and E_z in the equations are half a cell away from the $x = 1$ plane, as shown in Fig. 2.
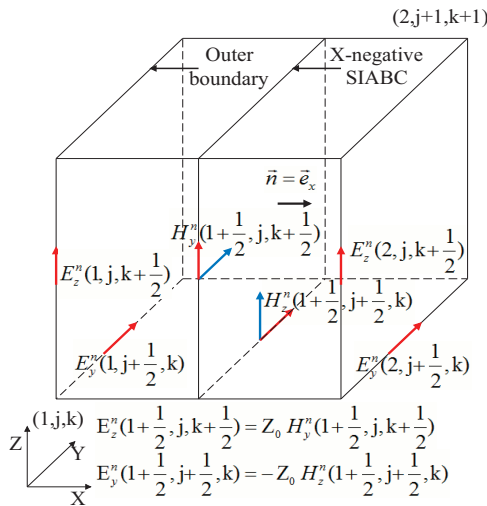
Fig. 2. SIABC for the X negative boundary.

One should notice that the indices, i, j, k are not exactly the same in the figures and formulas. Table 2 lists the relationship between these indices.

Table 2: Correspondences of indices in figures and updating equations

Fomulations	Figures
$E_x(i,j,k)$	$E_x(i+1/2,j,k)$
$E_y(i,j,k)$	$E_y(i,j+1/2,k)$
$E_z(i,j,k)$	$E_z(i,j,k+1/2)$
$H_x(i,j,k)$	$H_x(i,j+1/2,k+1/2)$
$H_y(i,j,k)$	$H_y(i+1/2,j,k+1/2)$
$H_z(i,j,k)$	$H_z(i+1/2,j+1/2,k)$

Since both H_y^n and H_z^n can be approximated using time difference with:

$$
\begin{cases}
H_y^n = \dfrac{1}{2}[H_y^{n+1/2} + H_y^{n-1/2}], \\
H_z^n = \dfrac{1}{2}[H_z^{n+1/2} + H_z^{n-1/2}].
\end{cases}
$$

Then equations (7b) and (7c) of this X negative plane become:

$$
\begin{cases}
H_y^{n+\frac{1}{2}}(1,j,k) = \dfrac{1 - \frac{dtZ_0}{\mu_y \triangle x}}{1 + \frac{dtZ_0}{\mu_y \triangle x}} H_y^{n-\frac{1}{2}}(1,j,k) \\
\quad + \dfrac{\frac{2dt}{\mu_y \triangle x}}{1 + \frac{dtZ_0}{\mu_y \triangle x}} E_z^n(2,j,k) - \dfrac{\frac{dt}{\mu_y \triangle z}}{1 + \frac{dtZ_0}{\mu_y \triangle x}} \\
\quad [E_x^n(1,j,k+1) - E_x^n(1,j,k)], \\
\qquad\qquad\qquad\qquad\qquad\qquad\qquad (8) \\
H_z^{n+\frac{1}{2}}(1,j,k) = \dfrac{1 - \frac{dtZ_0}{\mu_z \triangle x}}{1 + \frac{dtZ_0}{\mu_z \triangle x}} H_z^{n-\frac{1}{2}}(1,j,k) \\
\quad - \dfrac{\frac{2dt}{\mu_y \triangle x}}{1 + \frac{dtZ_0}{\mu_z \triangle x}} E_y^n(2,j,k) + \dfrac{\frac{dt}{\mu_z \triangle y}}{1 + \frac{dtZ_0}{\mu_z \triangle x}} \\
\quad [E_x^n(1,j+1,k) - E_x^n(1,j,k)].
\end{cases}
$$

The above equations for calculating $H_y^{n+\frac{1}{2}}$ and $H_z^{n+\frac{1}{2}}$ are in the same form as those used in the normal source-free FDTD method as listed in [10], which are:

$$
\begin{cases}
H_y^{n+\frac{1}{2}}(i,j,k) = C_{hyh} H_y^{n-\frac{1}{2}}(i,j,k) \\
\quad + C_{hyez}(E_z^n(i+1,j,k) - E_z^n(i,j,k)) \\
\quad - C_{hyex}(E_x^n(i,j,k+1) - E_x^n(i,j,k)), \\
\qquad\qquad\qquad\qquad\qquad\qquad\qquad (9) \\
H_z^{n+\frac{1}{2}}(i,j,k) = C_{hzh} H_y^{n-\frac{1}{2}}(i,j,k) \\
\quad + C_{hzex}(E_x^n(i,j+1,k) - E_x^n(i,j,k)) \\
\quad - C_{hzey}(E_y^n(i+1,j,k) - E_y^n(i,j,k)).
\end{cases}
$$

One should point out that for $i = 1$, the $E_z(1,j,k)$ and $E_y(1,j,k)$ remains 0 during the entire updating process. Thus, it is obvious that the only difference between SIABC and normal FDTD updating equations is the expression of the C coefficients for the tangential magnetic field components on the boundary.

The formulas of SIABC for the other five boundaries can be derived using the same procedure.

For the SIABC on the X positive boundary, the geometry of this case is shown in Fig. 3, and the corresponding updating equations for this case are given as:

$$
\begin{cases}
H_y^{n+\frac{1}{2}}(nx,j,k) = \dfrac{1-\frac{dtZ_0}{\mu_y\triangle x}}{1+\frac{dtZ_0}{\mu_y\triangle x}}H_y^{n-\frac{1}{2}}(nx,j,k) \\[3mm]
\quad - \dfrac{\frac{2dt}{\mu_y\triangle x}}{1+\frac{dtZ_0}{\mu_y\triangle x}}E_z^n(nx,j,k) - \dfrac{\frac{dt}{\mu_y\triangle z}}{1+\frac{dtZ_0}{\mu_y\triangle x}} \\[3mm]
\quad [E_x^n(nx,j,k+1) - E_x^n(nx,j,k)], \\[3mm]
H_z^{n+\frac{1}{2}}(nx,j,k) = \dfrac{1-\frac{dtZ_0}{\mu_z\triangle x}}{1+\frac{dtZ_0}{\mu_z\triangle x}}H_z^{n-\frac{1}{2}}(nx,j,k) \\[3mm]
\quad + \dfrac{\frac{2dt}{\mu_y\triangle x}}{1+\frac{dtZ_0}{\mu_z\triangle x}}E_y^n(nx,j,k) + \dfrac{\frac{dt}{\mu_z\triangle y}}{1+\frac{dtZ_0}{\mu_z\triangle x}} \\[3mm]
\quad [E_x^n(nx,j+1,k) - E_x^n(nx,j,k)].
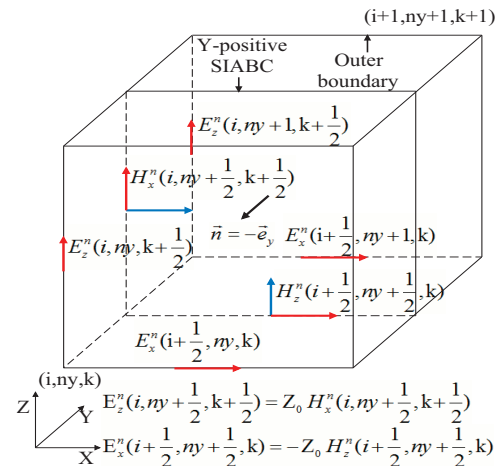\end{cases}
\tag{10}
$$
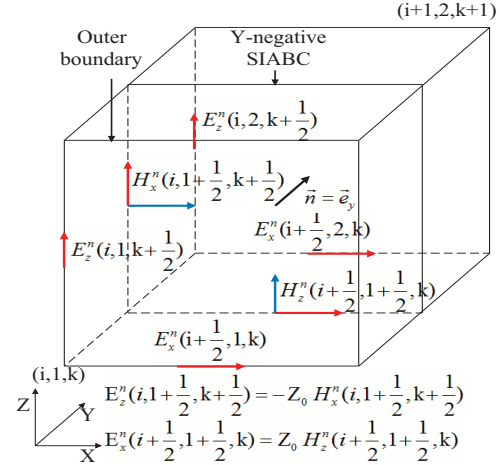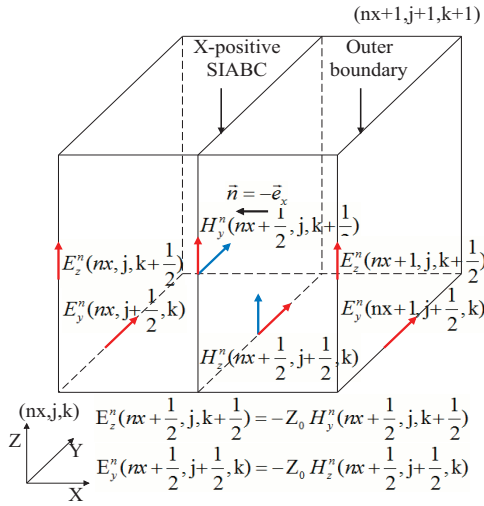
Fig. 3. SIABC for the X positive boundary.

For the SIABC on the Y negative boundary, the geometry of this case is shown in Fig. 4, and the updating equations for this case are given as:

$$
\begin{cases}
H_x^{n+\frac{1}{2}}(i,1,k) = \dfrac{1-\frac{dtZ_0}{\mu_x\triangle y}}{1+\frac{dtZ_0}{\mu_x\triangle y}}H_x^{n-\frac{1}{2}}(i,1,k) \\[3mm]
\quad - \dfrac{\frac{2dt}{\mu_x\triangle y}}{1+\frac{dtZ_0}{\mu_y\triangle y}}E_z^n(i,2,k) + \dfrac{\frac{dt}{\mu_x\triangle z}}{1+\frac{dtZ_0}{\mu_x\triangle y}} \\[3mm]
\quad [E_y^n(i,1,k+1) - E_y^n(i,1,k)], \\[3mm]
H_z^{n+\frac{1}{2}}(i,1,k) = \dfrac{1-\frac{dtZ_0}{\mu_z\triangle y}}{1+\frac{dtZ_0}{\mu_z\triangle y}}H_z^{n-\frac{1}{2}}(i,1,k) \\[3mm]
\quad + \dfrac{\frac{2dt}{\mu_z\triangle y}}{1+\frac{dtZ_0}{\mu_z\triangle y}}E_x^n(i,2,k) + \dfrac{\frac{dt}{\mu_z\triangle x}}{1+\frac{dtZ_0}{\mu_z\triangle y}} \\[3mm]
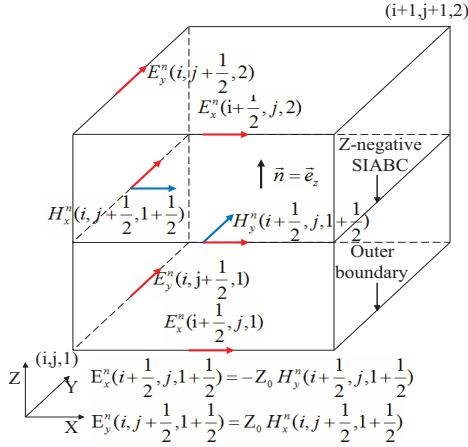\quad [E_y^n(i+1,1,k) - E_y^n(i,1,k)].
\end{cases}
\tag{11}
$$

Fig. 4. SIABC for the Y negative boundary.

For the SIABC on the Y positive boundary, the geometry of this case is shown in Fig. 5, and the updating equations for this case are given as:

$$
\begin{cases}
H_x^{n+\frac{1}{2}}(i,ny,k) = \dfrac{1-\frac{dtZ_0}{\mu_x\triangle y}}{1+\frac{dtZ_0}{\mu_x\triangle y}}H_x^{n-\frac{1}{2}}(i,ny,k) \\[3mm]
\quad + \dfrac{\frac{2dt}{\mu_x\triangle y}}{1+\frac{dtZ_0}{\mu_y\triangle y}}E_z^n(i,ny,k) + \dfrac{\frac{dt}{\mu_x\triangle z}}{1+\frac{dtZ_0}{\mu_x\triangle y}} \\[3mm]
\quad [E_y^n(i,ny,k+1) - E_y^n(i,ny,k)], \\[3mm]
H_z^{n+\frac{1}{2}}(i,ny,k) = \dfrac{1-\frac{dtZ_0}{\mu_z\triangle y}}{1+\frac{dtZ_0}{\mu_z\triangle y}}H_z^{n-\frac{1}{2}}(i,ny,k) \\[3mm]
\quad - \dfrac{\frac{2dt}{\mu_z\triangle y}}{1+\frac{dtZ_0}{\mu_z\triangle y}}E_x^n(i,ny,k) + \dfrac{\frac{dt}{\mu_z\triangle x}}{1+\frac{dtZ_0}{\mu_z\triangle y}} \\[3mm]
\quad [E_y^n(i+1,ny,k) - E_y^n(i,ny,k)].
\end{cases}
\tag{12}
$$

Fig. 5. SIABC for the Y positive boundary.

For the SIABC on the Z negative boundary, the geometry of this case is shown in Fig. 6, and the updating equations for this case are given as:

$$
\begin{cases}
H_x^{n+\frac{1}{2}}(i,j,1) = \dfrac{1 - \frac{dtZ_0}{\mu_x \triangle z}}{1 + \frac{dtZ_0}{\mu_x \triangle z}} H_x^{n-\frac{1}{2}}(i,j,1) \\[2mm]
+ \dfrac{\frac{2dt}{\mu_x \triangle z}}{1 + \frac{dtZ_0}{\mu_y \triangle z}} E_y^n(i,j,2) + \dfrac{\frac{dt}{\mu_x \triangle y}}{1 + \frac{dtZ_0}{\mu_x \triangle z}} \\[2mm]
[E_z^n(i,j+1,1) - E_z^n(i,j,1)], \\[2mm]
H_y^{n+\frac{1}{2}}(i,j,1) = \dfrac{1 - \frac{dtZ_0}{\mu_y \triangle z}}{1 + \frac{dtZ_0}{\mu_y \triangle z}} H_y^{n-\frac{1}{2}}(i,j,1) \\[2mm]
- \dfrac{\frac{2dt}{\mu_y \triangle z}}{1 + \frac{dtZ_0}{\mu_y \triangle z}} E_x^n(i,j,2) + \dfrac{\frac{dt}{\mu_y \triangle x}}{1 + \frac{dtZ_0}{\mu_y \triangle z}} \\[2mm]
[E_z^n(i+1,j,1) - E_z^n(i,j,1)].
\end{cases}
\tag{13}
$$

Fig. 6. SIABC for the Z negative boundary.

For the SIABC on the Z positive boundary, the geometry of this case is shown in Fig. 7, and the updating equations for this case are given as:

$$
\begin{cases}
H_x^{n+\frac{1}{2}}(i,j,nz) = \dfrac{1 - \frac{dtZ_0}{\mu_x \triangle z}}{1 + \frac{dtZ_0}{\mu_x \triangle z}} H_x^{n-\frac{1}{2}}(i,j,nz) \\[2mm]
- \dfrac{\frac{2dt}{\mu_x \triangle z}}{1 + \frac{dtZ_0}{\mu_y \triangle z}} E_y^n(i,j,nz) + \dfrac{\frac{dt}{\mu_x \triangle y}}{1 + \frac{dtZ_0}{\mu_x \triangle z}} \\[2mm]
[E_z^n(i,j+1,nz) - E_z^n(i,j,nz)], \\[2mm]
H_y^{n+\frac{1}{2}}(i,j,nz) = \dfrac{1 - \frac{dtZ_0}{\mu_y \triangle z}}{1 + \frac{dtZ_0}{\mu_y \triangle z}} H_y^{n-\frac{1}{2}}(i,j,nz) \\[2mm]
+ \dfrac{\frac{2dt}{\mu_y \triangle z}}{1 + \frac{dtZ_0}{\mu_y \triangle z}} E_x^n(i,j,nz) + \dfrac{\frac{dt}{\mu_y \triangle x}}{1 + \frac{dtZ_0}{\mu_y \triangle z}} \\[2mm]
[E_z^n(i+1,j,nz) - E_z^n(i,j,nz)].
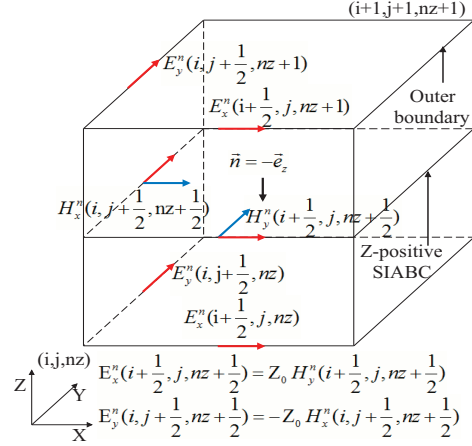\end{cases}
\tag{14}
$$

Fig. 7. SIABC for the Z positive boundary.

With these equations, one can now implement this SIABC in FDTD codes. It is also obvious from these equations that, compared to PML or CPML, the only thing needed to be done is to initialize the update coefficients for the tangential magnetic field components at the boundaries, no other changes are required in the FDTD codes when SIABC is used. That is really a great benefit specially for implementation on parallel or GPU hardware in order to accelerate the computations.

B. 2D SIABC formulation

The 2D problem is a simplification of the 3D problem. In a 2D problem, for example, a TM_z case, which is composed of E_z, H_x, H_y only, the formulas can be extracted from the 3D formulas easily. The geometry of a 2D problem is shown in Fig. 8 with designated SIABC boundaries.
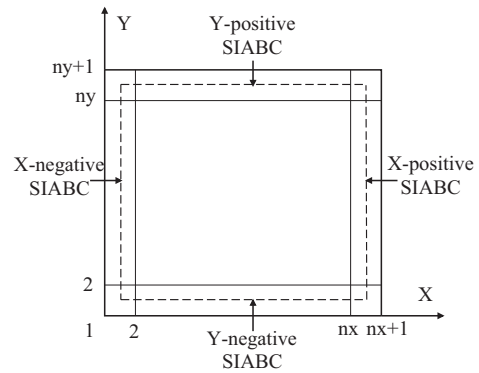

Fig. 8. Geometry of a 2D problem with SIABC boundaries.

For the SIABC on the X negative boundary,

the geometry of this case is illustrated in Fig. 9, and the updating equation is given as:

$$H_y^{n+1/2}(1,j) = \frac{\mu_y dx - Z_0 dt}{\mu_y dx + Z_0 dt} H_y^{n-1/2}(1,j)$$
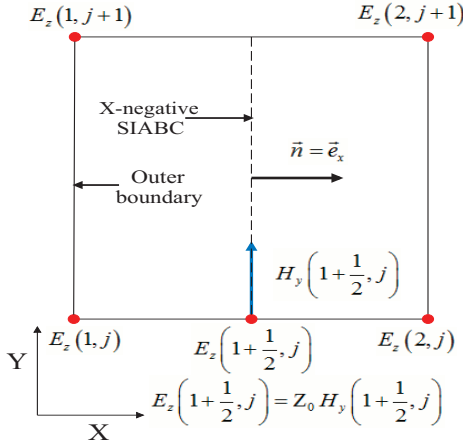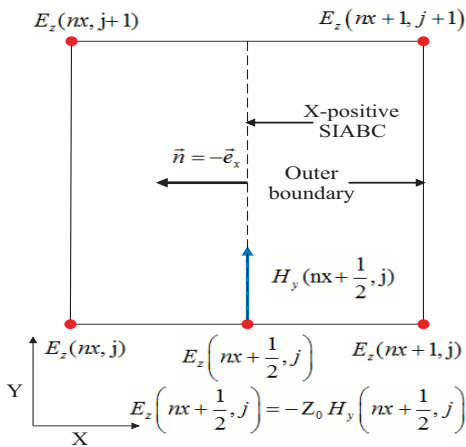$$+ \frac{2dt E_z^n(2,j)}{\mu_y dx + Z_0 dt}. \quad (15)$$

Fig. 9. SIABC for the X negative boundary.

For the SIABC on the X positive boundary, the geometry of this case is illustrated in Fig. 10, and the updating equation is given as:

$$H_y^{n+1/2}(nx,j) = \frac{\mu_y dx - Z_0 dt}{\mu_y dx + Z_0 dt} H_y^{n-1/2}(nx,j)$$
$$- \frac{2dt E_z^n(nx,j)}{\mu_y dx + Z_0 dt}. \quad (16)$$

Fig. 10. SIABC for the X positive boundary.

For the SIABC on the Y negative boundary, the geometry of this case is illustrated in Fig. 11,

and the updating equation is given as:

$$H_x^{n+1/2}(i,1) = \frac{\mu_x dy - Z_0 dt}{\mu_x dy + Z_0 dt} H_x^{n-1/2}(i,1)$$
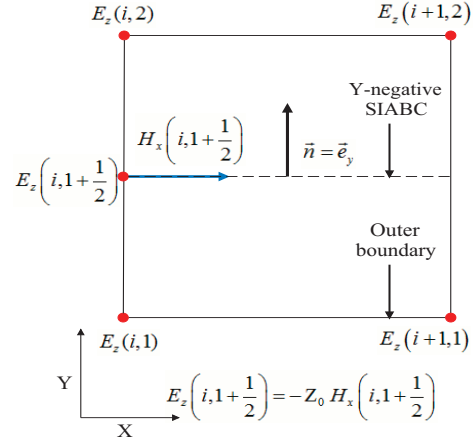$$- \frac{2dt E_z^n(i,2)}{\mu_x dy + Z_0 dt}. \quad (17)$$

Fig. 11. SIABC for the Y negative boundary.

For the SIABC on the Y positive boundary, the geometry of this case is illustrated in Fig. 12, and the updating equation is given as:

$$H_x^{n+1/2}(i,ny) = \frac{\mu_x dy - Z_0 dt}{\mu_x dy + Z_0 dt} H_x^{n-1/2}(i,ny)$$
$$+ \frac{2dt E_z^n(i,ny)}{\mu_x dy + Z_0 dt}. \quad (18)$$
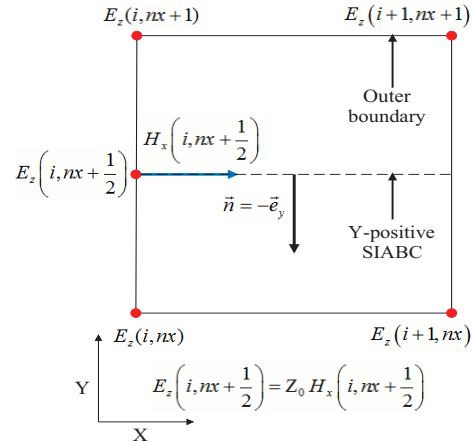

Fig. 12. SIABC for the Y positive boundary.

C. 1D SIABC formulation

The 1D problem is also a simplification of the 2D problem. In a one dimensional case there is no variation in the problem geometry and field

distributions in 2 of the coordinate dimensions. For instance, if there are only E_z and H_y, as shown in Fig. 13, and the wave propagates in the X direction, the corresponding FDTD updating equations can be derived as below:

For the SIABC on the X negative boundary,

$$H_y^{n+1/2}(1) = \frac{\mu_0 dx - Z_0 dt}{\mu_0 dx + Z_0 dt} H_y^{n-1/2}(1)$$
$$+ \frac{2dt}{\mu_0 dx + Z_0 dt} E_z^n(2). \quad (19)$$

For the SIABC on the X positive boundary,

$$H_y^{n+1/2}(nx) = \frac{\mu_0 dx - Z_0 dt}{\mu_0 dx + Z_0 dt} H_y^{n-1/2}(nx)$$
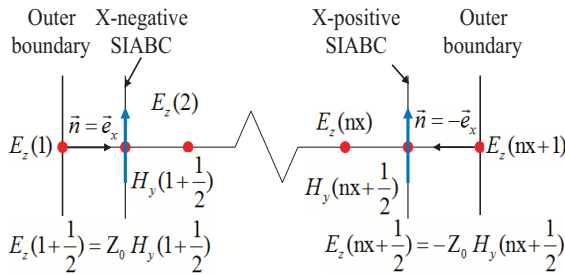$$- \frac{2dt}{\mu_0 dx + Z_0 dt} E_z^n(nx). \quad (20)$$

Fig. 13. Geometry of a 1D problem with SIABC boundaries.

III. VERIFICATION EXAMPLES AND RESULTS

In this section, a few examples are discussed. All examples except the first and the last are similar to those in [10] where the CPML parameters were selected for optimum CPML performance.

A. Dipole radiation near a sphere

In a 3D problem, a dipole antenna is located 20 cells away from a dielectric sphere of radius = $10mm$, whose parameters are $\epsilon = 3, \mu = 1, \sigma = 0$. The cell size of this problem is $\triangle x = \triangle y = \triangle z = 1mm$. Components of the electric field are sampled 20 cells away from the sphere center, at 11 different points, designated $P1$ to $P11$, as shown in Fig. 14. The dipole antenna is activated with a Gaussian pulse. For the absorbing boundary condition with 10-layers of CPML, the air buffer between the objects (in this case, the dielectric sphere) inside the problem space and the outer boundaries is 15 cells. For the SIABC absorbing boundary condition,

the air buffer is varying from 30 cells to 50 cells, since the distance between the scattering objects and SIABC can affect the performance of SIABC greatly.

S(0,0,0), P1(0,10,0), P2(0,16,14), P3(0,30,20)
P4(0,44,14), P5(0,50,0), P6(20,30,0), P7(10,20,14)
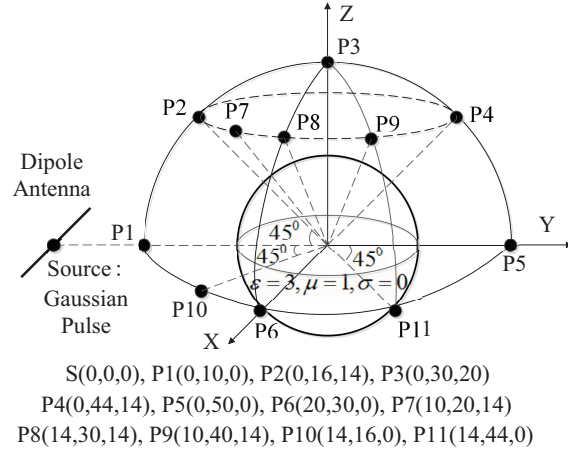P8(14,30,14), P9(10,40,14), P10(14,16,0), P11(14,44,0)

Fig. 14. Geometry of the 3D problem.

Table 3 lists the time needed for the simulations when applying SIABC and 10-layers CPML.

Table 3: Time needed for the simulations using Matlab with 1000 time steps

ABCs	Number of Air Buffer	Time (m)
CPML(10)	15	2.2737
SIABC	25	1.8138
SIABC	30	2.5159
SIABC	50	7.9297

Table 4 lists the maximum percentage difference of field values from SIABC compared to those from 10-layers CPML in time domain and frequency domain separately, with the number of air buffer between the scattering objects and SIABC changing. The percentage difference is calculated according to:

$$Differ = \frac{|E_{SIABC} - E_{CPML}|}{max(|E_{CPML}|)} \times 100\%, \quad (21)$$

where E_{SIABC} refers to the magnitude of sampled electric field when the ABC is SIABC, E_{CPML} refers to the magnitude of sampled electric field when the ABC is 10-layers CPML.

As listed in Table 4, point P4 has the largest maximum difference among all sample points. Figure 15 shows the sampled electric field at point P4 in time and frequency domains.

Table 4: Maximum percentage difference between SIABC and 10-layers CPML

Point	25 Cells		30 Cells		50 Cells	
	Time	Freq	Time	Freq	Time	Freq
P1	1.51	2.222	1.03	1.34	0.33	0.46
P2	1.80	2.74	1.07	1.58	0.45	0.57
P3	5.79	7.38	3.83	3.40	1.39	2.65
P4	19.05	11.78	13.15	6.94	4.28	2.96
P5	17.00	11.40	11.44	9.69	3.63	2.22
P6	6.08	6.24	3.70	5.00	2.11	3.08
P7	3.14	4.35	2.11	2.07	0.60	0.70
P8	6.98	6.25	4.60	3.30	1.04	1.25
P9	13.35	11.47	9.38	5.87	2.43	2.80
P10	3.79	5.51	2.98	2.83	1.41	1.47
P11	7.48	6.11	6.51	4.26	2.88	3.46

(a)

(b)
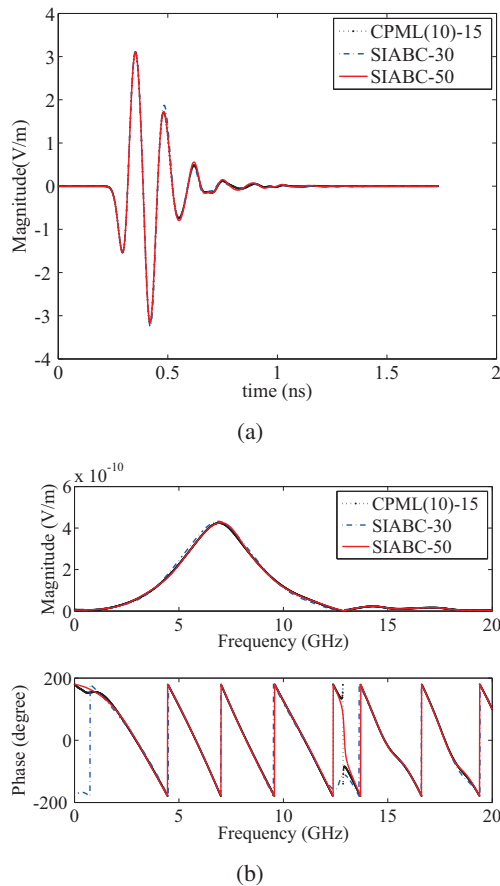
Fig. 15. Sampled E_x at P4 in (a) time domain; (b) frequency domain.

B. Microstrip low-pass filter

For this problem, the space is composed of cells with $\triangle x = 0.4064mm$, $\triangle y = 0.4233mm$,

$\triangle z = 0.265mm$. An air gap of 5 cells is left between the filter and the outer boundary in the xn, xp, yn, yp, zn and zp direction. The substrate is $3 \times \triangle z$ thick and has a relative dielectric constant of 2.2. The microstrip filter is terminated by a voltage source with 50Ω internal resistance on one end and by a 50Ω on the other end. The voltage is excited by a Gaussian waveform. The FDTD problem space is illustrated in Fig. 16.
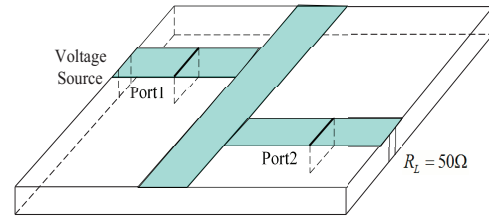

Fig. 16. A microstrip low pass filter geometry.

In the CPML case, the boundaries are terminated by 10 cells of CPML, and the number of cells between the CPML and the filter is 5. In the SIABC case, the air gap surrounding the filter is changing from 10 to 80.

Table 5 lists the maximum percentage difference based on the SIABC relative to those of the CPML values. It is obvious that the performance of SIABC with 30 cells air buffer is already quite acceptable compared to the performance of the CPML.

Table 5: Maximum percentage difference of S-parameters based on SIABC relative to those based on 10-layers CPML

Air Gap	S_{11} Difference	S_{21} Difference
20	7.4654 (5.02 GHz)	13.361 (8.38 GHz)
30	2.1921 (5.02 GHz)	2.2190 (8.30 GHz)
40	1.2828 (11.06 GHz)	1.1573 (8.32 GHz)
50	1.7183 (11.10 GHz)	0.5650 (8.32 GHz)
60	1.2654 (11.06 GHz)	0.7433 (8.32 GHz)
70	0.9164 (11.10 GHz)	0.7001 (8.32 GHz)
80	0.6800 (11.08 GHz)	0.8002 (8.32 GHz)

Figures 17 and 18 show the calculated S_{11} and S_{21} of the low pass filter when the absorbing boundary condition is set as CPML and SIABC.
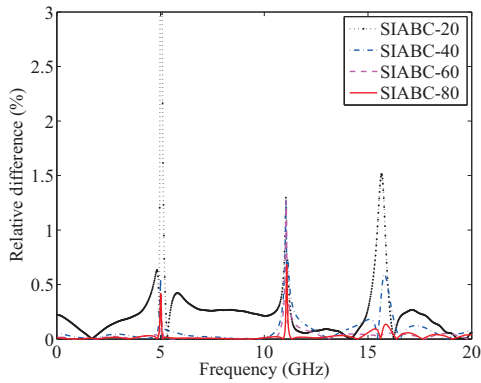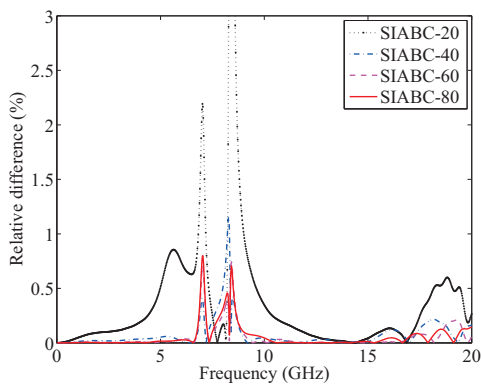
Fig. 17. Percentage difference of S_{11}.

Fig. 18. Percentage difference of S_{21}.

C. Scattering from a dielectric sphere

Figure 19 shows an FDTD problem space including a dielectric sphere illuminated by an x polarized plane wave travelling in the positive z direction. The problem space is divided into cells with size $\triangle x = 0.75cm, \triangle y = 0.75cm$, and $\triangle z = 0.75cm$. The dielectric sphere has a radius of 10 cm, relative permittivity of 3, and relative permeability of 2. The waveform of the plane wave is Gaussian. The RCS is calculated from the FDTD simulations at 1 GHz.

Figures 20 and 21 display the normalized RCS when the absorbing boundary condition is 10-layers CPML and SIABC, respectively. The exact RCS of this dielectric sphere is also calculated as presented in [11] and is shown in the figure.

Here, the number of cells of air buffer is 10 for the CPML case, and for the SIABC case, it is ranging from 20 to 40. The maximum percentage error of RCS based on 10-layers CPML and SIABC relative to analytic solution is listed in Table 6.
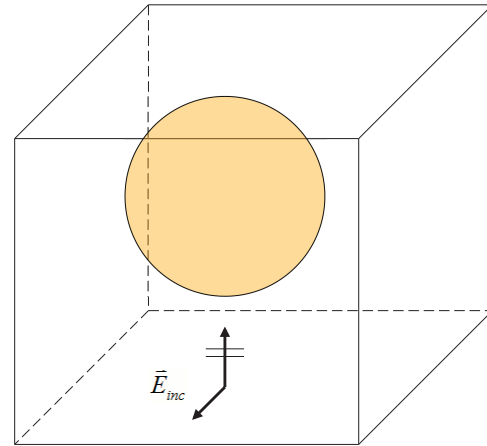

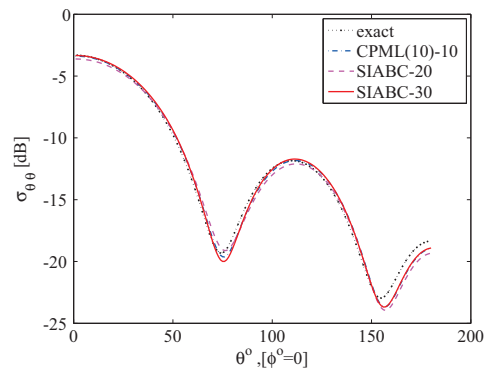Fig. 19. A FDTD problem space including a dielectric sphere.

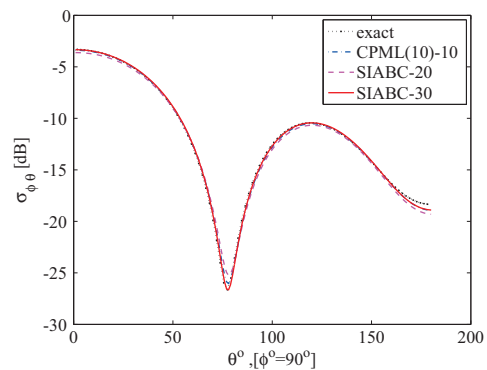Fig. 20. RCS_θ at 1 GHz in the xz plane compared with the analytical solution.

Fig. 21. RCS_ϕ at 1 GHz in the yz plane compared with the analytical solution.

One can draw from the figures and the table that when the air buffer between SIABC and the dielectric sphere is larger than 30 cells, the

performance of SIABC is in the same order as that of 10-layers CPML.

Table 6: Maximum percentage error of RCS based on 10-layers CPML and SIABC relative to analytic solution

ABCs	Air Buffer	RCS_θ	RCS_ϕ
CPML(10)	10	4.1483	2.5428
SIABC	20	5.5099	5.2008
SIABC	30	3.6534	2.1599
SIABC	40	3.5760	3.6353

D. Radiation from a patch antenna

In this example, a patch antenna is used to examine the performance of SIABC. A microstrip rectangular square patch antenna is constructed, as shown in Fig. 22. The problem space identified with grid size $\triangle x = 2mm, \triangle y = 2mm, \triangle z = 0.95mm$. A rectangular brick in the problem space representing the substrate of the antenna with dimensions of $60mm \times 40mm \times 1.9mm$ and dielectric constant of 2.2. A PEC plate as the ground of the antenna is placed right under the bottom side of the substrate covering its entire surface area. A PEC patch sits on the top surface of the substrate with $56mm$ width and $20mm$ length in the x and y directions, respectively. The patch is centred on the top surface of the substrate. The feeding point to the patch is in the middle point of the long edge of the patch. A voltage source with 50Ω internal resistance between the ground plane and the feeding point is used. This patch antenna operates at 3.45 GHz.
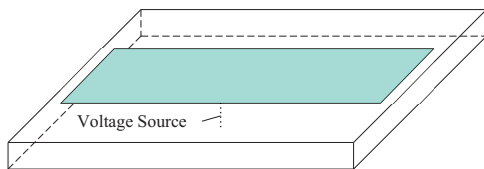

Fig. 22. A microstrip patch antenna geometry.

Table 7 lists the maximum percentage difference of SIABC results relative to those of the 10-layers CPML. The number of cells of the air buffer for the CPML case is 10, while for the SIABC case, it is ranging from 20 to 50.

Figures 23 and 24 compare the performance when using 10-layers CPML and SIABC.

Table 7: Maximum difference of directivity based on SIABC relative to those based on 10-layers CPML

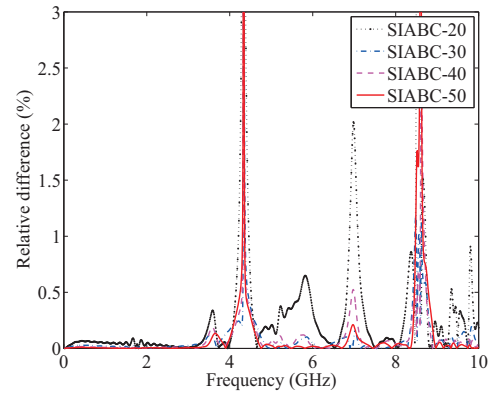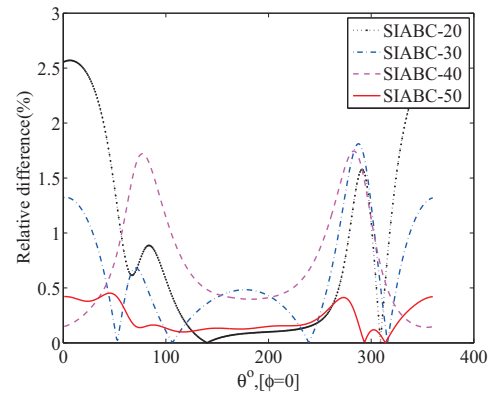| Air Buffer	Directivity Difference
20	2.5859
30	1.8525
40	1.7813
50	0.4508

Fig. 23. Relative difference of S_{11}.

Fig. 24. Relative difference of directivity in xz plane.

E. Absorbing performance in a 1D problem

For a one dimensional problem, a Gaussian pulse is generated in the middle of a problem space of 1m length. Here, the cell size is $\triangle x = 1mm$. One side of the problem space is terminated by PML, and the other side by SIABC. Thus, the performance of PML and SIABC can be easily compared in time domain right after the first reflection from both sides. The geometry of this problem is shown in Fig. 25.
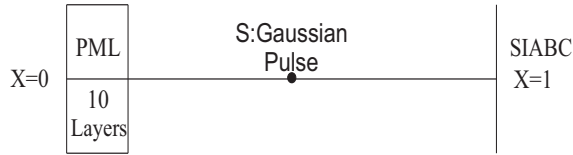
Fig. 25. Geometry of a 1D problem with PML (left) and SIABC (right) boundaries.

The result shown in Fig. 26 indicates that the reflected wave when using SIABC is 4 times smaller than that when using 10 layers of PML.
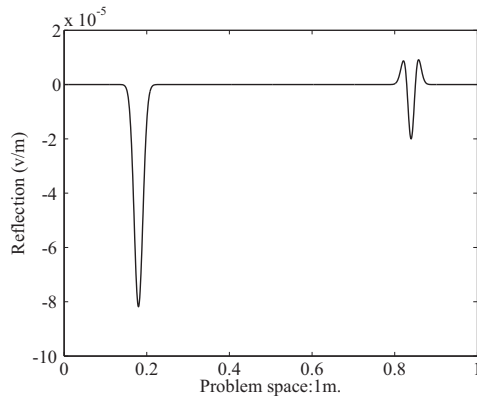

Fig. 26. Comparison of reflection from PML (left) and SIABC (right) boundaries.

IV. MEMORY USAGE

In this section, the memory usage of 10-layers CPML and SIABC is compared for a 3D computational domain. In order to simplify the analysis, the number of cells of the domain in x, y, and z directions are all the same. The relative memory increase due to the required air buffer cells when using SIABC relative to 10-layers CPML is computed as follows:

$$M_{increase} = \frac{M_{SIABC} - M_{CPML}}{M_{CPML}} \times 100\%. \quad (22)$$

Figure 27 illustrates the comparison of memory usage for domain sizes reaching one billion cells.

For practical size problems it is clear that the extra memory required is not prohibitive. Furthermore, it should be pointed out that the use of the non-uniform discretization for the free space between the objects and the outer boundary will drastically reduce the usage of this extra memory. Results based on this approach will be reported soon.
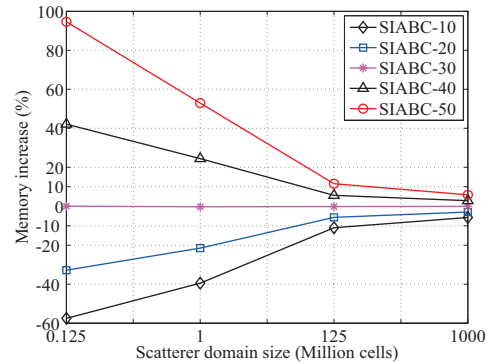

Fig. 27. Memory usage of SIABC relative to 10-layers CPML.

V. CONCLUSION

In this paper, a novel absorbing boundary condition, SIABC is introduced. Formulas of SIABC in 3D, 2D, and 1D are derived and implemented for FDTD method. From the formulations one can find out that this ABC is extremely easy to implement. The performance of SIABC is compared to that of 10-layers PML in 1D and 10-layers CPML in 3D. All the results show that when the distance between the objects inside the computational and the SIABC is in the order of 50 cells, SIABC can achieve a comparable or better results than those based on CPML results.

REFERENCE

[1] B. Engquist and A. Majda, "Absorbing boundary conditions for numerical simulation of waves," *Proceedings of the National Academy of Sciences*, vol. 74, no. 5, pp. 1765–1766, 1977.

[2] G. Mur, "Absorbing boundary conditions for the finite-difference approximation of the time-domain electromagnetic-field equations," *Electromagnetic Compatibility, IEEE Transactions on*, no. 4, pp. 377–382, 1981.

[3] J. P. Berenger, "A perfectly matched layer for the absorption of electromagnetic waves," *Journal of Computational Physics*, vol. 114, no. 2, pp. 185–200, 1994.

[4] J. A. Roden and S. D. Gedney, "Convolutional PML (CPML): an efficient fdtd implementation of the cfs-pml for arbitrary media," *Microwave and Optical Technology Letters*, vol. 27, no. 5, pp. 334–338, 2000.

[5] T. B. Senior, J. L. Volakis, and S. R. Legault, "Higher order impedance and absorbing boundary conditions," *Antennas and Propagation, IEEE Transactions on*, vol. 45, no. 1, pp. 107–114, 1997.

[6] S. Rytov, "Calcul du skin-effect par la méthode des perturbations," *J. Phys. USSR*, vol. 2, no. 3, pp. 233–242, 1940.

[7] M. Leontovich, "Approximate boundary conditions for the electromagnetic field on the surface of a good conductor," *Investigations on Radiowave Propagation*, vol. 2, pp. 5–12, 1948.

[8] J. G. Maloney and G. S. Smith, "The use of surface impedance concepts in the finite-difference time-domain method," *Antennas and Propagation, IEEE Transactions on*, vol. 40, no. 1, pp. 38–48, 1992.

[9] J. H. Beggs, R. J. Luebbers, K. S. Yee, and K. S. Kunz, "Finite-difference time-domain implementation of surface impedance boundary conditions," *Antennas and Propagation, IEEE Transactions on*, vol. 40, no. 1, pp. 49–56, 1992.

[10] A. Z. Elsherbeni and V. Demir, *The finite-difference time-domain method for electromagnetics with MATLAB simulations*. Raleigh, NC: SciTech Publishing Inc., 2009.

[11] V. Demir, A. Z. Elsherbeni, D. Worasawate, and E. Arvas, "A graphical user interface (GUI) for plane-wave scattering from a conducting, dielectric, or chiral sphere," *Antennas and Propagation Magazine, IEEE*, vol. 46, no. 5, pp. 94–99, 2004.